Manufacturing the current flow diverter architecture in REBCO tapes using silver inkjet printing

OPEN ACCESS
IOP Publishing
Superconductor Science and Technology
Supercond. Sci. Technol. **37** (2024) 125019 (9pp)
https://doi.org/10.1088/1361-6668/ad8e03

Manufacturing the current flow diverter architecture in REBCO tapes using silver inkjet printing

Haïfa Ben Saâd[1,2,*], **Christian Lacroix**[1,2,*], **Mariia Zhuldybina**[3] and **Frédéric Sirois**[1,*]

[1] Polytechnique Montreal, Montreal, QC H3C 3A7, Canada
[2] Boreal Conductors Inc., Montreal, QC H2S 2P9, Canada
[3] Institut des communications graphiques et de l'imprimabilité, Montreal, QC H2M 2E2, Canada

E-mail: haifa.ben-saad@polymtl.ca, christian.lacroix@polymtl.ca and f.sirois@polymtl.ca

Received 1 July 2024, revised 17 October 2024
Accepted for publication 1 November 2024
Published 22 November 2024

Abstract

A low normal zone propagation velocity (NZPV) combined with critical current inhomogeneities favor the nucleation of destructive hot spots in rare-earth barium copper oxide (REBCO) tapes. Increasing the NZPV using the current flow diverter (CFD) concept is a promising solution to mitigate the risk of developing hot spots. The fabrication method of CFD REBCO tapes implies several steps consisting in masking, silver etching, mask removal, and silver deposition, which takes time and remains a barrier to the implementation of a low-cost industrial production of long-length CFD REBCO tapes. This work presents a cost-effective and maskless CFD fabrication approach that relies on inkjet printing (IJP) of silver patterns directly on top of the REBCO layer to create a non-uniform interfacial resistance between the silver and the REBCO surface, along the width of the tape. The parameters of IJP and oxygen annealing were optimized to obtain highly conductive silver patterns deposited on the surface of the REBCO layer. CFD REBCO tapes were successfully fabricated using commercial REBCO tapes and the proposed method without degrading the superconducting properties. Experimental measurements revealed an increase of the NZPV by a factor of 6–7 compared to commercial REBCO tapes.

Keywords: current flow diverter (CFD), quench detection, high-temperature superconductors, inkjet printing, normal zone propagation velocity (NZPV).

1. Introduction

Rare-earth barium copper oxide (REBCO) coated conductors (CCs) are promising for high-field applications, such as fusion magnets [1], particle accelerators [2], and nuclear magnetic resonance imaging [3], due to their high critical temperature (T_c), high critical current density (J_c), and excellent mechanical properties [4–6]. However, one of the challenges faced by the applied superconductivity community is quench detection and protection of REBCO-based magnets. Traditionally, quench detection in low-temperature superconductor magnets relies on measuring the voltage at both ends or in different sections of the magnet coil. However, in high-temperature superconductor (HTS) magnets, the quench produces a very small voltage that increases so slowly that it may damage the coil before being detected by the quench detection system [7]. To circumvent this problem, several novel quench detection techniques have been proposed, based

* Authors to whom any correspondence should be addressed.

on either thermometry [8], magnetic hall sensors arrays [9], optical fibers [10] or radio frequency waves [11].

In a superconducting wire, the velocity at which a hot spot expands is called the normal zone propagation velocity (NZPV). In REBCO tapes, the NZPV at 77 K and in self-field is approximately $2 - 40\,\mathrm{cm\,s^{-1}}$. This low NZPV, coupled with critical current inhomogeneities along the length, increases the risk of developing destructive hot spots. A possible solution is to increase the NZPV with the current flow diverter (CFD) concept [12]. The CFD concept consists in modifying the architecture of REBCO tapes by patterning a high interfacial resistance between the REBCO layer and the silver layer to increase the NZPV. As a consequence, this increases the rising rate of the voltage at the ends of the tape in the same proportions and implies that a larger portion of the magnet is quenched [7, 13].

Over the years, several fabrication processes have been proposed to integrate the CFD architecture in REBCO tapes. The original approach consists in removing partially the silver layer on top of the REBCO layer using chemical etching. Silver is then redeposited on the REBCO layer using a physical method such as sputtering. One important drawback of this process is the loss of silver during the etching process [14]. Although several recycling methods can be used to recover the silver from the etching solution, exploring alternative approaches remains relevant to lower the cost and promote the industrialization of the CFD architecture [15].

An alternative technique that has been explored consisted in deliberately reducing the thickness of the silver layer to create the so-called b-CFD architecture [16]. In this work, a process based on the sulfurization of the upper part of the silver layer was used, thus creating Ag_2S, in order to reduce the thickness of the pure silver layer while avoiding the corrosion of the REBCO layer with sulfur and a degradation of the critical current. However, further work to ensure the quality of the contacts for current injection with this approach is required.

Another technique consisted in the deposition of a thin oxide layer at the REBCO/silver interface to create a high interfacial resistance [17]. A cerium oxide layer (Ce_xO) was deposited on top of the oxygenated REBCO layer before silver deposition. An additional annealing in an oxygen atmosphere was performed to reduce the interfacial resistance created by the Ce_xO layer. However, it was observed that the critical current of the REBCO tape was degraded during the oxygen annealing due to a change in the stoichiometry of the REBCO layer, where barium atoms were forced to diffuse out of the REBCO layer through the cracks of the Ce_xO layer.

A different approach consisted in using the inkjet printing (IJP) of a yttrium oxide (Y_2O_3) layer on top of a pre-oxygenated REBCO layer, followed by a silver deposition and an additional annealing in an oxygen atmosphere [18]. Electrical characterization revealed the successful implementation of the CFD architecture, but the overall interfacial resistance was in the range of $100\,\mu\Omega.\mathrm{cm}^2$, which is too high for practical applications. Furthermore, the complexity of this approach makes it unattractive for an industrial production.

In the most recent approach to create the CFD architecture, a locally controlled diffusion reaction between evaporated indium and the silver layer was used to form a stable intermetallic compound (IMC) throughout the whole thickness of the silver layer down to the REBCO/silver interface [19]. This Ag–In IMC at the interface acted as a CFD layer, leading to an increase of the NZPV. While this approach is rather simple to implement in a fabrication process, it is likely to add an extra cost to REBCO tapes production considering that indium is an expensive metal. Furthermore, more investigations on the effects of this Ag-In IMC interlayer in REBCO tapes remain to be done, especially regarding current injection.

In this work, we explore a different approach to create the CFD architecture, which consists in the direct writing of silver patterns on the REBCO surface using IJP, which is now possible thanks to the commercial availability of conductive inks formulated with metallic silver [20, 21]. An oxygen annealing treatment is performed to reduce the interfacial resistance between the IJP silver and the REBCO layer. Afterwards, a silver layer is deposited using sputtering to cover the whole REBCO layer. This approach has the advantage that it requires no chemical etching or masking steps. In addition, it does not introduce additional species in the REBCO tape.

The first section of the paper describes the experimental methodology used to create the silver patterns with IJP. The second section discusses the structural and electrical properties of the silver printed patterns. The last section presents the fabrication and electrical characterization of IJP CFD tapes.

2. Experimental procedure

2.1. REBCO tape samples

Samples used in this work are commercial REBCO tapes obtained from THEVA Dünnschichttechnik GmbH, Superconductor Technologies Inc. (STI), and SuperPower Inc. (SP). The THEVA tapes consisted in a 12 mm wide and 100 μm thick Hastelloy substrate (C-276^{TM}) on which a 3.1 μm thick buffer layers stack was deposited. A 3.1 μm thick GdBaCuO layer was grown on top of the buffer layer [22]. The GdBaCuO layer of these THEVA tapes was not annealed in an oxygen atmosphere, and not coated with a silver layer. These tapes were used to perform preliminary IJP testing. The layered structure of commercial STI tapes consisted of a 50 μm thick Hastelloy (C-276^{TM}) substrate, a 0.58–0.78 μm thick buffer layers stack, and a 1 μm thick GdBaCuO layer. Finally, there was a 2 μm thick silver layer on top of the GdBaCuO layer only (no silver on the substrate side) [17]. Commercial SP tapes comprised a 50 μm thick Hastelloy (C-276^{TM}) substrate, a 0.2 μm thick buffer layers stack, and a 1.6 μm thick Zr-doped GdBaCuO layer. The whole architecture was surrounded with a total of 2 μm of silver (1 μm on both sides) [23]. Both the STI and SP tapes were 4 mm wide. The critical current of the tapes at 77 K and in self-field was 100 A to 110 A for the STI tapes, and 140 A to 150 A for the SP tapes.

For clarity purposes, the unmodified commercial STI and SP samples will be called 'regular' tapes, while the modified tapes that include the CFD architecture fabricated using IJP will be called 'IJP CFD' tapes.

2.2. Inkjet printing

A Dimatix inkjet printer (DMP-2831) was used to deposit conductive silver patterns on the outer surface of the REBCO layer. The 16-jet Dimatix materials cartridge, designed for high-resolution and non-contact jetting, contained 16 nozzles. During printing, the samples were fixed on a vacuum plate whose temperature was adjusted to 70° C.

The Novacentrix JS-A291 ink was chosen considering its good adhesion on the REBCO layer and viscosity. Silver lines having a width of 0.5–1 mm and a thickness of 3.8 μm were printed. Critical current measurements revealed no degradation in the critical current of the samples after printing the silver lines with this ink.

2.3. Microstructure characterization

A Dektak 150 surface profiler was used to determine the average thickness of the printed lines for different oxygen annealing temperatures. The microstructural properties of the printed patterns were also investigated using a scanning electron microscope (SEM) equipped with a field emission gun (FEG SEM; JOEL7600TFE). For that matter, a stair-step cut was created in 4 mm × 4 mm sample pieces using a focused ion beam instrument (Hitachi FIB-2000A). Then, the samples were cleaned and mounted on a sample holder using carbon tape. The acceleration voltage was 10 kV and the working distance was 10.7 mm. Samples were tilted to an angle of approximately 30° to face the secondary electron detector. Finally, a chemical composition analysis was performed using energy dispersive spectroscopy (EDS) [24, 25].

2.4. Electrical characterization

A four-point method was used to determine the room-temperature resistivity of the printed patterns vs. annealing temperature. The same method was used to obtain the resistance of IJP CFD REBCO tapes from 77 to 285 K [17].

The critical current I_c ($E_c = 1\ \mu\text{V cm}^{-1}$) and the NZPV of IJP CFD REBCO tapes were measured in a liquid nitrogen bath at ambient pressure and in self-field. A pulsed current source was used to generate square current pulses lasting a few milliseconds. Up to 40 pogo pins placed every 1.27 mm were used to measure the voltage across the length of the sample. For the NZPV measurements, an NdFeB magnet was used to reduce locally the critical current to create a normal zone. More details about the measurement setup are available in [14].

To measure the interfacial resistance between the silver and the REBCO layer, a 10 cm long sample was divided into two 5 cm long parts. In each part, the REBCO layer was exposed in two locations by chemical etching of the top silver layer and using a shadow mask to cover three silver pads. After etching, both parts were soldered facing each other with indium at one pad of each sample termination. The remaining pads were used to inject the current into the sample and to install voltage taps on each part to measure the voltage drop. More details about the experimental setup are presented in [17].

3. Inkjet printed silver lines on REBCO surface

3.1. Fabrication details

To obtain uniform silver lines, several tests were carried out using the Dimatix 2831 IJP system to set the optimal spacing D between the drops and the pulse voltage, which controls the resolution of the printed patterns. The pulse voltage is the voltage amplitude applied to the piezoelectric part in the printhead to generate the required pressure for ejecting ink droplets on the substrate, thus controlling the size and the velocity of the ink droplets. The tests consisted in printing 1 mm wide lines on THEVA samples without a top silver layer. Figure 1 presents images of the silver lines for $D = 15$, 17 and 20 μm. Uniform continuous silver patterns were only obtained with $D = 15\ \mu$m, while for $D = 17\ \mu$m and 20 μm, the printed tracks were divided into separate lines. Also, different values of the pulse voltage were tested and it was found that the optimal pulse voltage was 16 V.

To ensure a good adhesion of the printed silver ink on the REBCO surface, samples were cured at 100° C for 45 min in an ambient atmosphere. This step was followed by an oxygen annealing at temperatures between 300° C and 500° C to decrease the interfacial resistance between the printed silver and the REBCO layer [26]. After annealing, the adhesion of silver on the REBCO surface was verified using adhesive tape peel tests. No silver particles were found on the tape, indicating that the adhesion of silver on REBCO was good.

3.2. Microstructural characterization

Figure 2 presents the cross-sectional views of five printed silver lines on the surface of the REBCO layer of THEVA tapes after curing at 100° C for 45 min: (a) before oxygen annealing, (b) after a one-hour oxygen annealing at 300° C, (c) after a one-hour oxygen annealing at 400° C, (d) after a one-hour oxygen annealing at 500° C and (e) after a one-hour oxygen annealing at 400° C followed by the deposition by sputtering of a one-micron thick silver layer. In figure 2(a), the silver deposited by IJP presents multiple voids (black areas in the Ag layer), which was confirmed by EDS mapping (not shown). Figure 3 presents magnified images of figures 2(a) and (b). A thin interspace is visible between the REBCO layer and the printed silver, which suggests a poor adhesion of the silver to the REBCO surface. Following annealing in an oxygen atmosphere, a progressive agglomeration of the silver particles is observed. The size of the grains becomes larger, and the pore density is reduced, as the annealing temperature increases from 300 to 500° C. Furthermore, no interspace at the printed silver/REBCO interface is visible after oxygen annealing at 300° C or above. In figure 2(e), while no voids are present in

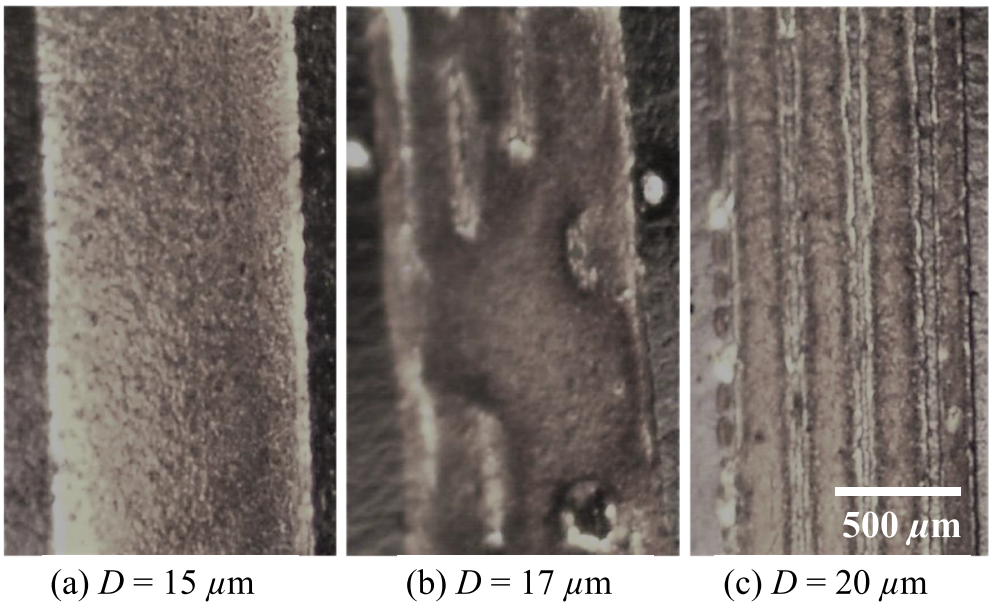

Figure 1. Images of printed silver lines on REBCO tapes for a drop spacing of (a) $D = 15\ \mu$m, (b) $D = 17\ \mu$m, and (c) $D = 20\ \mu$m.

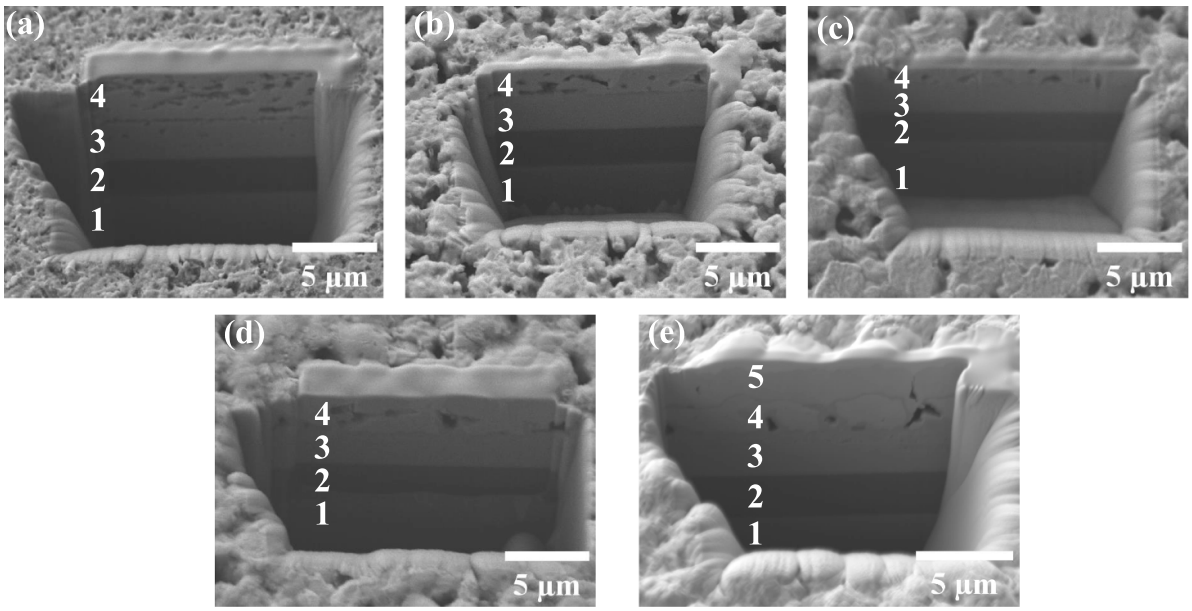

Figure 2. Cross-sectional views of Ag printed lines on THEVA tapes cured at 100° C for 45 min: (a) before oxygen annealing, (b) after a one-hour oxygen annealing at 300° C, (c) after a one-hour oxygen annealing at 400° C, (d) after a one-hour oxygen annealing at 500° C and (e) after a one-hour oxygen annealing at 400° C and followed by the deposition by sputtering of a one-micron thick silver layer. The numbers refer to the different layers of the REBCO tape, namely (1) the substrate, (2) the buffer layers, (3) the REBCO layer, (4) the printed silver, and (5) the sputtered silver.

the sputtered silver layer, confirming its good quality, voids are still present in the silver deposited by IJP.

Figure 4 displays the thickness profiles of a 1 mm wide silver line before and after annealing at 300° C for one hour in an oxygen atmosphere. It reveals that the line has shrunk after the heat treatment, which can be attributed to the coalescence of silver nanoparticles during annealing, as observed in figures 2(b)–(d). The average thicknesses of a silver line before and after annealing at 300° C, 400° C, and 500° C are presented in figure 5, where we observe that it decreases as the annealing temperature increases.

3.3. *Electrical resistivity*

Figure 5 presents the variation of the silver resistivity vs. annealing temperature. Before annealing, the resistivity of

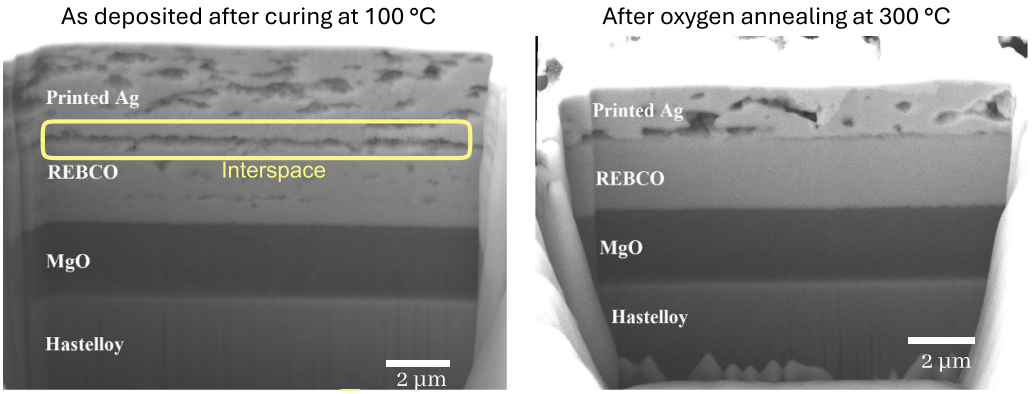

Figure 3. Magnified cross-sectional views of Ag printed lines on THEVA tapes cured at 100° C for 45 min: (a) before oxygen annealing, (b) after a one-hour oxygen annealing at 300° C.

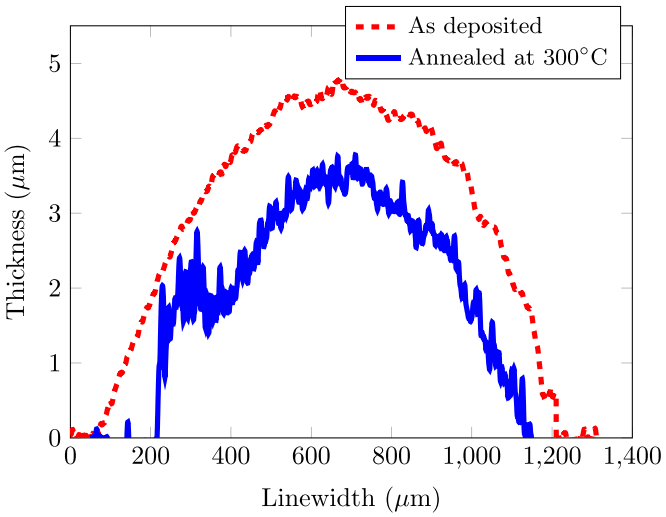

Figure 4. Thickness profiles of printed silver lines before (dashed red line) and after a one-hour annealing at 300° C in an oxygen atmosphere (solid blue line).

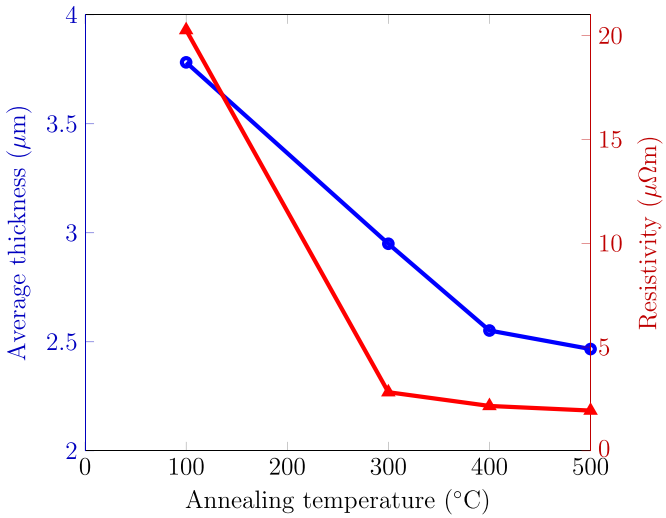

Figure 5. Average thickness (blue) and measured resistivity (red) of printed silver lines vs. annealing temperature.

the silver line is 20.3 $\mu\Omega$.cm, and drops to 1.9 $\mu\Omega$.cm after annealing at a temperature of 500° C, which is of the same order of magnitude as the resistivity of pure silver (1.6 $\mu\Omega$.cm). This drop in the resistivity can be explained by the evaporation of organic components and by an increase in the mass density of silver (reduction in the void volume). The decrease in the electrical resistivity of inkjet-printed silver patterns and the coalescence of silver nanoparticles after employing heat treatment has also been reported in previous studies [27, 28].

4. Inkjet printing of CFD tapes

4.1. Fabrication details

To fabricate IJP CFD tapes, commercial STI and SP samples were used. The fabrication steps of the IJP CFD tapes are described in figure 6. Firstly, the silver layer on the REBCO layer was removed using chemical etching with a solution of NH_4OH:H_2O_2:H_2O;1:1:4. A high interfacial resistance is created at the silver/REBCO interface when the REBCO is exposed to the ambient atmosphere or/and to a chemical solution of silver etching [29, 30]. Then, a 3.8 μm thick and 0.5 mm wide silver line was printed locally on the REBCO surface. The CFD coverage fraction f, which is 1 minus the ratio between the width of the printed line and the total width of the tape, was thus 0.875. The sample was then annealed in an oxygen atmosphere at 400° C for one hour. This heat treatment decreased the contact resistance between the silver line created by IJP and the REBCO layer, although the exact value could not be measured. Finally, a 2 μm thick layer of silver, covering the whole surface of the STI and SP IJP CFD samples, was deposited by sputtering. The resulting architectures of the IJP CFD tapes are shown in figure 6.

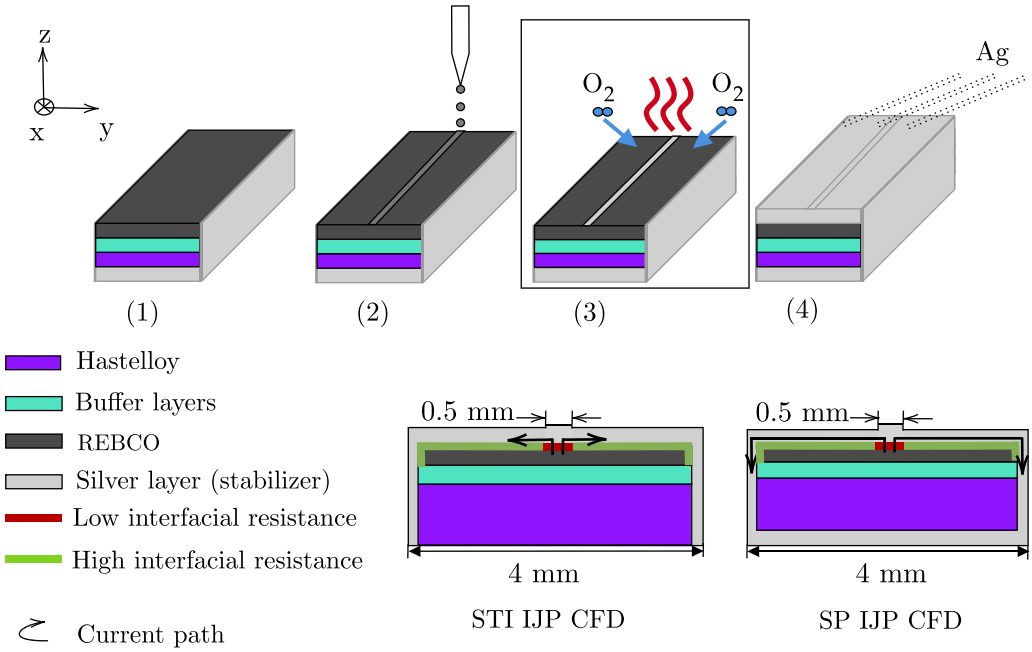

Figure 6. Top figures: CFD fabrication steps using IJP: (1) etching of the silver layer on top of the REBCO layer, (2) IJP of a silver line, (3) oxygen annealing, and (4) deposition of silver by sputtering. Bottom figures: the two CFD geometries fabricated by IJP are shown.

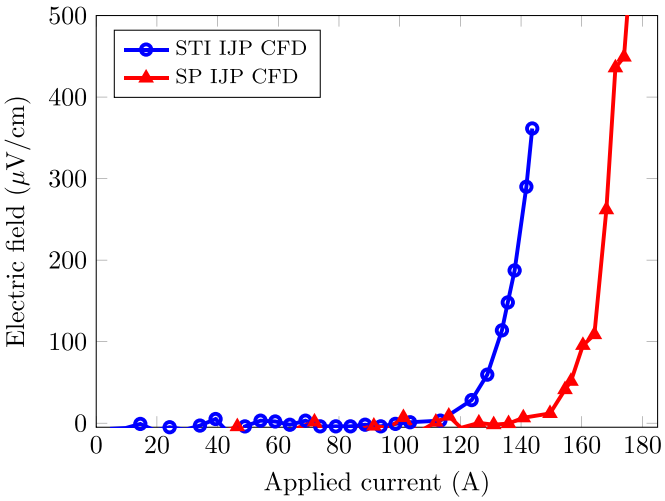

Figure 7. *E–I* curves of the STI IJP CFD sample (blue circles) and the SP IJP CFD sample (red triangles) measured at 77 K and in self-field.

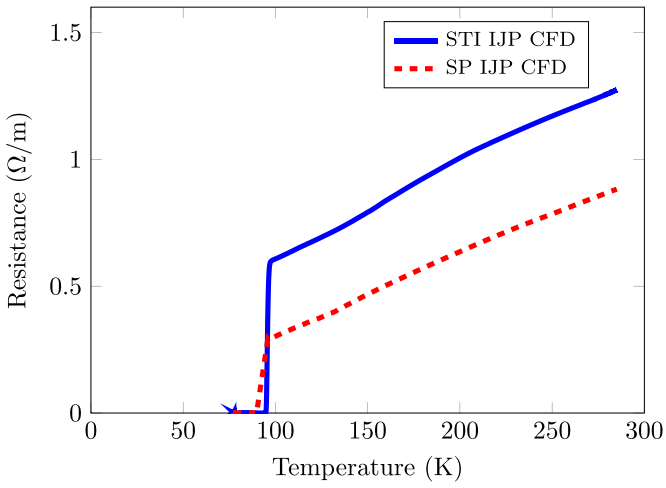

Figure 8. Resistance vs. temperature curves of the STI IJP CFD sample (solid blue line) and SP IJP CFD sample (dashed red line).

4.2. Critical current and temperature dependence of the resistance

The critical current of the IJP CFD tapes was measured in liquid nitrogen at ambient pressure (77 K) and in self-field. Figure 7 shows the *E–I* curves for both IJP CFD samples. The values for the critical currents are 96 A for the STI IJP CFD sample and 141 A for the SP IJP CFD sample, while the *n*-factors are 22 and 26, respectively. The temperature dependence of the electrical resistance of the samples for an applied current of 100 mA was also measured and is shown in figure 8. The critical temperatures are 94 K and 92 K for the STI IJP CFD and the SP IJP CFD samples, respectively, which are the same as that of the regular (i.e. unmodified) REBCO tapes. The SP IJP CFD sample has a surrounding silver layer of a total thickness of 3 μm, while the STI IJP CFD sample has only a 2 μm thick top silver layer. Since the SP IJP CFD sample has a greater quantity of silver, it has a lower normal state resistance above the critical temperature.

4.3. Interfacial resistance measurements

The interfacial resistance R_i^* of STI IJP CFD and SP IJP CFD samples was measured at 77 K. A R_i^* of 33 $\mu\Omega.\text{cm}^2$ was obtained for the STI IJP CFD sample and 35 $\mu\Omega.\text{cm}^2$ for the SP

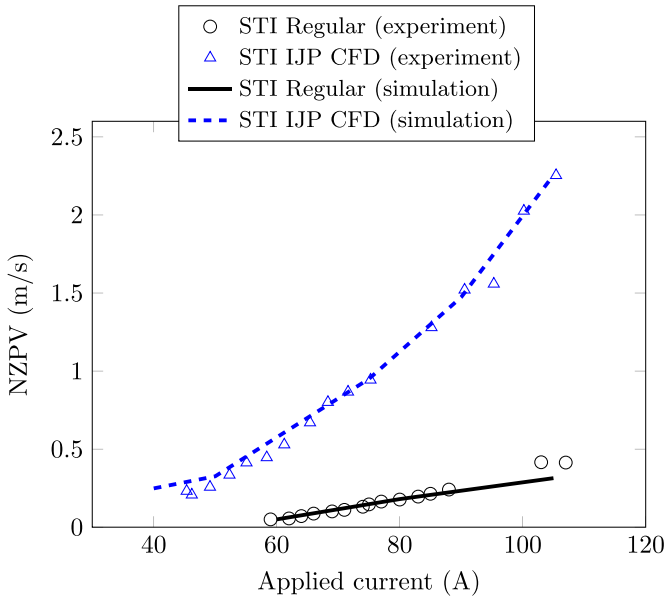

Figure 9. Measured NZPV values vs. the applied current for a STI regular sample (black circles) and a STI IJP CFD sample (blue triangles). The solid black line corresponds to the simulated NZPV for a STI regular sample, while the dashed blue line is the simulated NZPV for a STI IJP CFD sample for $R_i^* = 33\,\mu\Omega.\text{cm}^2$.

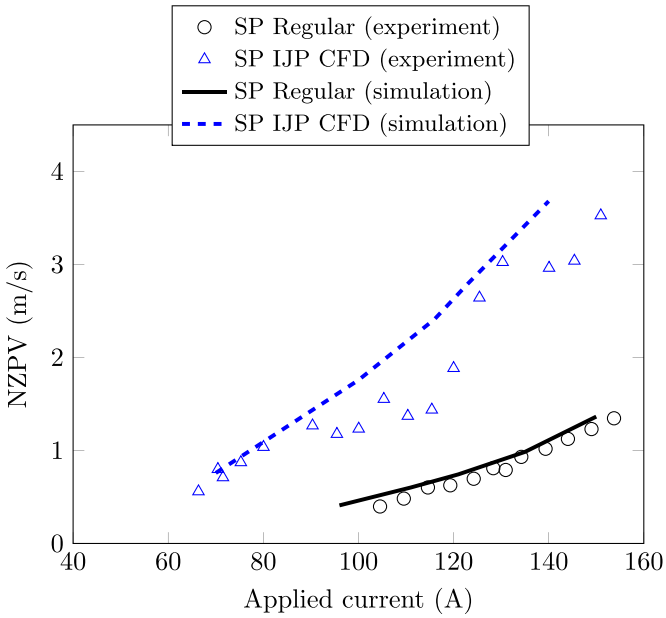

Figure 10. Measured NZPV values vs. the applied current for a SP regular sample (black circles) and a SP IJP CFD sample (blue triangles). The solid black line corresponds to the simulated NZPV for a SP regular sample, while the dashed blue line is the simulated NZPV for a SP IJP CFD sample for $R_i^* = 35\,\mu\Omega.\text{cm}^2$.

IJP CFD sample. These values represent the effective interfacial resistance of the whole REBCO/silver interface containing the CFD part (high interfacial resistance) and the low interfacial resistance part.

Typical values of interfacial resistance in regular (commercial) REBCO tapes range between 0.02 and 0.1 $\mu\Omega.\text{cm}^2$ [31, 32]. According to previous works, the interfacial resistance of CFD tapes with a coverage fraction f of 0.9 is 0.8 $\mu\Omega.\text{cm}^2$ [12], which is lower than the interfacial resistance obtained for IJP CFD samples. This indicates that the interfacial resistance between the printed silver line and the REBCO layer in IJP CFD samples is higher than the low interfacial resistance part of conventional CFD samples [30].

4.4. Normal zone propagation velocity

The NZPV of both the STI and SP IJP CFD samples were measured in self-field and at 77 K and are presented in figures 9 and 10, respectively. For the STI IJP CFD sample, the NZPV was increased by a factor of 6–7 compared to the STI regular sample.

For the SP IJP CFD sample, the NZPV was increased by a factor of 3–4 compared to the SP regular sample. However, the SP regular sample had a total silver thickness of 2 μm while the SP IJP CFD sample had a 3 μm thick silver layer, which explains why the gain is only a factor of 3–4. Typically, for the same amount of stabilizer, the CFD architecture enhances the NZPV by a factor of approximately 7. The data points of the NZPV for the SP IJP CFD sample are scattered, probably because of current crowding in the center of the tape combined with voltage taps arranged in a 'zig zag'. This 'zig zag' type of arrangement had to be used due to the geometrical constraints of the SP IJP CFD sample (the sample was not long enough to use a different sample holder).

4.5. Numerical model

The NZPV of IJP CFD samples and regular samples were calculated using 3D finite element simulations based on the Electric Currents and Heat Transfer in Solids modules available in the COMSOL Multiphysics 5.5 software (see [12] for further details about the model). In this model, the thermal and electrical equations are interconnected through the Joule losses term. Adiabatic conditions were assumed (no heat exchange between the tape and the environment). The geometries of the samples, as depicted in figure 6, were implemented in the model. To increase the computational efficiency, the number of elements was reduced by taking advantage of the symmetries in the problem. Due to their small thickness, the stack of buffer layers and the resistive interface between the REBCO layer and the silver layer were reduced to thin-shell elements.

The electrical conductivity of the REBCO layer was expressed as two conductances in parallel, where one conductance corresponds to the normal state of REBCO (σ_n) and the second to the superconducting state of REBCO (σ_{sc}), modeled by a power-law, which is expressed as

$$\sigma_{sc}(T) = \frac{J_c(T)}{E_c}\left(\frac{||\vec{E}||}{E_c}\right)^{\frac{1-n(T)}{n(T)}}, \qquad (1)$$

$$J_c(T) = \begin{cases} J_{c0}\left(\frac{T_c - T}{T_c - T_0}\right) & \text{for } T < T_c, \\ 0 & \text{for } T \geqslant T_c, \end{cases} \quad (2)$$

$$n(T) = \begin{cases} (n_0 - 10)\left(\frac{T_c - T}{T_c - T_0}\right) + 10 & \text{for } T < T_c, \\ 10 & \text{for } T \geqslant T_c, \end{cases} \quad (3)$$

where $||\vec{E}||$ is the norm of the electric field, E_c is the electric field criterion (10^{-4} V m^{-1}), J_{c0} is the critical current density at T_0, n_0 is the power-law index at T_0, T_c is the critical temperature and T_0 is the operating temperature (77 K).

The temperature dependence of the electrical resistivity of silver was deduced from figure 8. It was assumed that the electrical resistivity was the same for the printed silver and the sputtered silver. The remaining material properties were available in the literature [12].

Numerical simulations using the experimental values $R_i^* = 33\ \mu\Omega.\text{cm}^2$ and $R_i^* = 35\ \mu\Omega.\text{cm}^2$ were performed to obtain the NZPV of the STI IJP CFD and SP IJP CFD samples, respectively. The value of the high interfacial resistance part (R_f), which is located between the sputtered silver and the REBCO layer, is typically between 100 $\mu\Omega.\text{cm}^2$ and 320 $\mu\Omega.\text{cm}^2$ [19, 30], which depends on the etching process and the time duration of the exposure of the REBCO layer to the ambient atmosphere. Using an iterative procedure, it was found that $R_f = 250\ \mu\Omega.\text{cm}^2$ was optimal for both STI and SP IJP CFD tapes. Similarly, the interfacial resistance between the printed silver layer and the REBCO layer R_i was optimized, and values of $R_i = 4.7\ \mu\Omega.\text{cm}^2$ for the STI IJP CFD sample and $R_i = 4.9\ \mu\Omega.\text{cm}^2$ for the SP IJP CFD sample were obtained, assuming

$$\frac{1}{R_i^*} = \frac{1-f}{R_i} + \frac{f}{R_f}. \quad (4)$$

As observed in figures 9 and 10, the results from numerical simulations are in good agreement with the measured NZPV for both regular and IJP CFD samples.

Although the overall interfacial resistance using this CFD fabrication approach is higher than the typical value of CFD REBCO tapes fabricated using the conventional method (33 $\mu\Omega.\text{cm}^2$ vs. 0.8 $\mu\Omega.\text{cm}^2$), the CFD IJP process can be further optimized by increasing the annealing temperature to lower the interfacial resistance between the printed silver and the REBCO layer.

5. Conclusion

In this work, it was demonstrated that the CFD architecture can be implemented by depositing a narrow line of silver directly on the REBCO surface of a commercial tape. Starting from an oxygenated REBCO tape where silver has been etched chemically, the silver line was deposited using IJP, which was followed by an oxygen annealing and by the deposition by sputtering of a silver layer on the whole REBCO layer. It was shown that this CFD fabrication method was compatible with REBCO tapes from two different tape manufacturers, STI and SuperPower. No degradation of the critical current was observed in the IJP CFD tapes in comparison with regular (unmodified) REBCO tapes. Furthermore, the measured NZPV of the IJP CFD samples was several times higher than that of the regular samples, confirming the presence of the CFD effect.

Ultimately, this CFD fabrication process could be integrated in the traditional fabrication process of REBCO tapes used by manufacturers. Indeed, the silver IJP step could be easily inserted between the growth of the REBCO layer and the oxygenation step. In contrary to the original CFD fabrication method, no chemical etching and masking/demasking steps would be required, thus greatly simplifying the CFD fabrication process. Furthermore, IJP is a mature technology, widely used in various industries and large-scale production. Scaling up such a process into a reel-to-reel system could allow the continuous fabrication of the CFD architecture with high precision and repeatability and at a reasonable cost. To reach optimal performance, it is crucial to obtain a low interfacial resistance between the printed silver and the REBCO layer. This requires further optimization of the silver printing and annealing processes to improve the quality of the silver lines. Further work is essential to explore the annealing of printed silver at temperatures higher than 400°C to reduce the interfacial resistance. Also, further work might be required to optimize the oxygenation of a REBCO layer in the case where its surface is partially covered by silver.

Data availability statement

All data that support the findings of this study are included within the article (and any supplementary files).

Acknowledgments

This Project has received funding from the Canadian National Sciences and Engineering Research Council (NSERC), CMC Microsystems, and Mitacs.

ORCID iDs

Haïfa Ben Saâd https://orcid.org/0000-0002-1620-5364
Christian Lacroix https://orcid.org/0000-0002-1648-1879
Mariia Zhuldybina https://orcid.org/0000-0002-4638-2695
Frédéric Sirois https://orcid.org/0000-0003-0372-9449

References

[1] Hartwig Z S *et al* 2023 *IEEE Trans. Appl. Supercond.* **34** 0600316
[2] van Nugteren J, Kirby G, Murtomäki J, DeRijk G, Rossi L and Stenvall A 2018 *IEEE Trans. Appl. Supercond.* **28** 4008509
[3] Park D, Bascuñán J, Li Y, Lee W, Choi Y and Iwasa Y 2021 *IEEE Trans. Appl. Supercond.* **31** 4300206

[4] Sorbom B *et al* 2015 *Fusion Eng. Des.* **100** 378–405
[5] Uglietti D 2019 *Supercond. Sci. Technol.* **32** 053001
[6] Mitchell N *et al* 2021 *Supercond. Sci. Technol.* **34** 103001
[7] Marchevsky M 2021 *Instruments* **5** 27
[8] Marchevsky M, Hershkovitz E, Wang X, Gourlay S A and Prestemon S 2018 *IEEE Trans. Appl. Supercond.* **28** 8322238
[9] Weiss J, Teyber R, Marchevsky M and Van Der Laan D 2020 *Supercond. Sci. Technol.* **33** 105011
[10] Scurti F, Weiss J, Van Der Laan D and Schwartz J 2021 *Supercond. Sci. Technol.* **34** 035026
[11] Marchevsky M, Lee G, Teyber R and Prestemon S 2023 *IEEE Trans. Appl. Supercond.* **33** 9000206
[12] Lacroix C and Sirois F 2014 *Supercond. Sci. Technol.* **27** 035003
[13] Muto S, Fujita S, Tsuchiya K, Takemoto T, Ishii M, Iijima Y and Daibo M 2022 *IEEE Trans. Appl. Supercond.* **32** 4701605
[14] Lacroix C *et al* 2022 *Supercond. Sci. Technol.* **35** 055009
[15] Syed S 2016 *Waste Manage.* **50** 234–56
[16] Barusco P, Obradors X, Giguere J, Lacroix C, Sirois F, Granados X, Puig T and Obradors X 2023 *Supercond. Sci. Technol.* **36** 125005
[17] Fournier-Lupien J H, Lacroix C, Huh J, Masse J P, Bellemare J and Sirois F 2021 *Materialia* **15** 101029
[18] Barusco P *et al* 2022 *ACS Omega* **7** 15315–25
[19] Barusco P, Ben-Saad H, Horn-Bourque D, Lacroix C, Sirois F, Puig T, Gutiérrez J, Granados X and Obradors X 2024 *IEEE Trans. Appl. Supercond.* **34** 6600906
[20] Perelaer J, De Gans B J and Schubert U S 2006 *Adv. Mater.* **18** 2101–4
[21] Uttiya S, Bernini C, Vignolo M, Pallecchi I, Marré D, Siri A S and Pellegrino L 2017 *Thin Solid Films* **642** 370–6
[22] THEVA Dünnschichttechnik GmbH 2022 (available at: www.theva.com)
[23] *2G HTS Wire Specifications* SuperPower Inc., Furukawa Electric Co., Ltd., 2012 (Accessed June 2023) (available at : www.superpower-inc.com/specification.aspx)
[24] Hitachi FB-2000A FIB Instrumentation *Applied Chemical and Morphological Analysis Laboratory (ACMAL)* (Accessed May 2023) (available at: www.mtu.edu/acmal/shared-facilities/electron-optics/instrumentation/hitachi-fb-2000a-fib/)
[25] Scanning Electron Microscope (SEM) JEOL Ltd. *JEOL Ltd.* (Accessed May 2023) (available at: www.jeol.com/products/scientific/sem/)
[26] Ekin J W, Larson T, Bergren N F, Nelson A, Swartzlander A, Kazmerski L, Panson A and Blankenship B 1988 *Appl. Phys. Lett.* **52** 1819–21
[27] Fernandes I J, Aroche A F, Schuck A, Lamberty P, Peter C R, Hasenkamp W and Rocha T L 2020 *Sci. Rep.* **10** 8878
[28] Shen W, Zhang X, Huang Q, Xu Q and Song W 2014 *Nanoscale* **6** 1622–8
[29] Russek S E, Sanders S, Roshko A and Ekin J 1994 *Appl. Phys. Lett.* **64** 3649–51
[30] Lacroix C, Lapierre Y, Coulombe J and Sirois F 2014 *Supercond. Sci. Technol* **27** 055013
[31] Hayasaka R, Ito S and Hashizume H 2019 *IEEE Trans. Appl. Supercond.* **29** 1–5
[32] Bagrets N, Nast R, Fournier-Lupien J H, Sirois F, Celentano G and Weiss K P 2021 *IEEE Trans. Appl. Supercond.* **31** 1–8